Crystal growth and magnetic structure of ternary silicide $EuPd_3Si_2$

Shivani Sharma,[1,*] Masoud Mardani,[1] Keke Feng,[1] Kaya Wei,[1] Ryan Baumbach,[1] Qiang Zhang,[2] David J. Singh,[3] and Theo Siegrist[1,4]

[1]*National High Magnetic Field Laboratory, Tallahassee, Florida 32310, USA*
[2]*Neutron Scattering Division, Oak Ridge National Laboratory, Oak Ridge, Tennessee 37831, USA*
[3]*Department of Physics and Astronomy, University of Missouri, Columbia, Missouri 65211, USA*
[4]*Department of Chemical and Biomedical Engineering, FAMU-FSU College of Engineering, Tallahassee, Florida 32310, USA*

(Received 12 July 2022; revised 13 December 2022; accepted 30 January 2023; published 17 February 2023)

The hexagonal $CaCu_5$-type structure ($P6/mmm$) is the prototype for more than 100 ternary borides, gallides, and silicides, with general stoichiometry of RTM_3X_2 (R = lanthanide/alkaline earth; TM = transition metal; X = B, Ga, Si, Ge). We report the synthesis, crystal structure, and bulk magnetic properties of polycrystalline and single crystal samples of $EuPd_3Si_2$ and its nonmagnetic analog $SrPd_3Si_2$. Both compounds crystallize in the orthorhombic space group symmetry $Imma$ (no. 74, $Z = 2$, $oI12$) displaying pseudohexagonal symmetry. Ferromagnetic (FM) order of Eu^{2+} at $T_{C1} = 78$ K and a spin-reorientation transition at $T_{C2} = 5$ K appear as distinctive features in bulk magnetization, specific heat, and resistivity/resistance measurements. Neutron powder diffraction measurements on $EuPd_3Si_2$ confirm FM order of the Eu^{2+} spins below T_{C1}, with the spins aligned along the a axis below T_{C2}. Electronic band structure calculations corroborate the crystal structure and the FM state for $EuPd_3Si_2$, with a Pd d-band polarization in the same direction as the Eu $4f$ polarization, enhancing the observed spin moment.

DOI: 10.1103/PhysRevMaterials.7.023402

I. INTRODUCTION

More than 100 ternary borides, gallides, and silicides are known to crystallize in the $CaCu_5$-type structure, which can be further subdivided by the general chemical formula RTM_xX_y where $x + y = 5$ and R is either a lanthanide or alkaline earth atom, TM is a transition element, and X = B, Ga, Si, or Ge [1–10]. Most of the substitutional variants crystallize either in the hexagonal (symmetry $P6/mmm$) prototype structure with different Wykoff positions for TM and X, or a distorted orthorhombic ($ErRh_3Si_2$ type, symmetry $Imma$) pseudohexagonal structure or monoclinic structure in very few cases [1]. In particular, the systems containing rare earth elements present unique opportunities for strengthening our understanding of critical phenomena such as valence fluctuations, Kondo effect, superconductivity, crystal field effects, or complex magnetism [2,5,6,9,11]. For example, $CeCo_3B_2$ is nonmagnetic, but the isoelectronic $CeRh_3B_2$ has an anomalously high ferromagnetic (FM) ordering temperature T_C of 115 K [8,10]. $CeRu_3B_2$ and $CeOs_3B_2$ are superconducting at low temperature [2], while the monoclinic $CeIr_3B_2$ is a mixed-valent nonmagnetic material [9,10]. The Curie temperature T_C of $CeRh_3B_2$ exceeds even that of $GdRh_3B_2$, with a $T_C = 90$ K, whereas $LaRh_3B_2$ becomes superconducting below 2.5 K [10,11]. In silicides, a giant crystal-electric-field effect and complex magnetic behavior are also reported for single crystalline $CeRh_3B_2$ with multistep character of magnetic ordering, whereas $CeIr_3Si_2$ is a Kondo lattice [7]. Detailed synthesis and magnetic properties of rare earth ruthenium borides $LnRu_3B_2$ (Ln = La-Lu, Y, Th, or U) confirm that most members of these systems show either superconductivity or magnetic order [10]. Subsequently, a detailed study on the lanthanide-rhodium-silicide $LnRh_3Si_2$ (Ln = Y, La, Nd, Sm, Gd, Dy, Ho, Er) system was carried out [4]. However, to our knowledge, no $ErRh_3Si_2$-type silicides have been reported with Eu and Pd. The possible reason for this is discussed in the subsequent sections.

Here we report the synthesis, crystal structure, and physical properties including magnetization, specific heat, and electrical resistivity/resistance of single crystal and polycrystalline samples of $EuPd_3Si_2$ and its nonmagnetic analog $SrPd_3Si_2$. The bulk magnetization and specific heat measurements reveal long-range ordering of Eu^{2+} below $T_{C1} = 78$ K and an additional spin-reorientation transition at $T_{C2} = 5$ K. Based on magnetic entropy estimation using heat capacity data, it appears that the full entropy corresponding to a $J = 7/2$ state is recovered by 78 K and no spin fluctuations above the ordered state were observed, which is supported by a Curie-Weiss fit down to 80 K. The resistivity measurements confirm that the system is metallic, and the charge carrier scattering is reduced below T_{C1}. Neutron powder diffraction (NPD) measurements on polycrystalline $EuPd_3Si_2$ confirm the ferromagnetic ground state of this compound. Electronic band structure calculations using the PBE + U density functional within density functional theory corroborate the details of the crystal structure and the FM order of Eu^{2+} spins.

II. EXPERIMENTAL

Single crystals of $EuPd_3Si_2$ were first obtained as a byproduct in the Bridgeman growth of $EuPd_2Si_2$, where 2 g of Eu, Pd, and Si in the stoichiometric ratio of 1:2:2 were melted

*phy.shivanisharma@gmail.com

in an arc furnace. The as prepared ingots were placed in a tantalum tube (0.5-mm wall thickness and 5-mm diameter) and sealed under argon. The tubes were then placed in an rf Bridgeman setup and heated to 1350 °C. After lowering the crucible through the hot zone in 24 h, 1–3-mm size and silver colored single crystal of $EuPd_3Si_2$ and 0.5–1-mm size and golden colored single crystals of $EuPd_2Si_2$ were obtained, together with minor amounts of other phases. The $EuPd_3Si_2$ crystals were easily separated from the $EuPd_2Si_2$ due to their distinct color contrast. In addition, $TaSi_2$ and related phases formed, indicating that the initial melt with stoichiometry Eu : Pd : Si = 1 : 2 : 2 is unstable in a tantalum crucible at elevated temperatures. Polycrystalline samples of $EuPd_3Si_2$ and $SrPd_3Si_2$ were subsequently prepared from stoichiometric mixtures melted in an arc furnace in two steps: first, Pd and Si were melted and, then, Eu or Sr were added to the Pd-Si melt. The samples were annealed at 850 °C for two weeks in sealed quartz ampoules. Small (0.1–0.4 mm) single crystals of $EuPd_3Si_2$ and $SrPd_3Si_2$ were also extracted from these samples. It is hard to avoid the formation of multiple phases in polycrystalline samples and, therefore, the analysis of polycrystalline samples without the knowledge of the crystal structure of $EuPd_3Si_2$ is rendered difficult. This is possibly the reason that previous literature does not describe this phase. For the present paper, we first grew the single crystals and used the crystallographic information in the multiphase fit of the powder data.

The phase purity of the polycrystalline samples was checked by powder x-ray diffraction (XRD) using a Scintag PAD-V x-ray diffractometer with Cu-Kα radiation and diffracted beam analyzer. Single crystals were characterized with an Oxford Diffraction Xcalibur-2 CCD diffractometer prior to physical property measurements. The crystal structure was solved using the CRYSTALS suite of programs [12]. Powder XRD patterns were fitted using a two-phase model. The bulk magnetization measurements were carried out in a Quantum Design magnetic property measuring system superconducting quantum interference device magnetometer, and specific heat and resistivity were measured with a Quantum Design physical property measuring system as a function of temperature and magnetic field. NPD measurements were performed using the POWGEN beamline at Oak Ridge National Laboratory. The neutron diffraction data were recorded at $T = 150$, 67, 30, and 1.6 K with 4 h of data collection at each temperature, using a center wavelength of 0.8 Å to cover a d range of 0.2–7 Å. Neutron experiments on compounds containing natural Eu are challenging due to the very large absorption cross section of Eu [13–15]. To minimize absorption, a short neutron wavelength was used, together with a small sample quantity ($\approx$1 g) placed in a POWGEN automatic changer (PAC) container with a very narrow diameter of 3 mm. An orange cryostat was used as the sample environment to cover the temperature between 1.6 and 300 K. The representational analysis was carried out using SARAH [16] to explore all the possible allowed magnetic structures and the BILBAO crystallographic suite of programs [17] was used for the magnetic symmetry analysis. The Rietveld refinements of the XRD and NPD data were performed using FULLPROF [18].

Density functional theory (DFT) calculations of the electronic structure employed the general potential linearized augmented plane-wave method as implemented in the WIEN2K code [19], using the generalized gradient approximation of Perdew, Burke, and Ernzerhof (PBE-GGA) [20] with addition of a Coulomb U of 6 eV with the fully localized limit to the Eu $4f$ orbitals. This removed the Eu $4f$ states from the vicinity of the Fermi energy. The calculations included the spin polarized FM alignment of the Eu moments. LAPW sphere radii were 1.90 bohrs for Si and 2.45 bohrs for Sr, Eu, and Pd. We used well converged basis sets defined by $R_{\min}K_{\max} = 7$, where $R_{\min} = 1.90$ bohrs is the smallest sphere radius and $K_{\max}$ is the plane-wave sector cutoff. This yields an effective $RK_{\max}$ above 9 for the metal atoms. The calculations are based on dense sampling of the Brillouin zone with $42 \times 42 \times 42$ grids for $EuPd_3Si_2$ and $SrPd_3Si_2$. Transport property calculations were done using the BOLTZTRAP code [21]. The results shown were obtained in a scalar relativistic approximation using the experimental lattice parameters, with atomic positions relaxed by total energy minimization. Calculations with inclusion of spin orbit coupling confirm that the orbital moments are very small ($\approx$–0.01 μ_B/Eu) justifying the scalar relativistic approximation.

III. RESULTS AND DISCUSSION

A. Room temperature structural characterization

The room temperature crystal structure of $EuPd_3Si_2$ based on the hexagonal $CaCu_5$ has the distorted pseudohexagonal symmetry of the $ErRh_3Si_2$-type structure [1]. The structure deviates from the $CaCu_5$ prototype by a small distortion in the $CaCu_5$ ab plane (approximate lattice parameters ratio $a/b = 1.754 \approx \sqrt{3}$), followed by doubling of the c axis. The initial C centering is lost, while an I centering is retained, doubling the original primitive unit cell volume. Of the initial symmetry elements, the mirror symmetry and the glide mirror planes are retained. To arrive at the standard setting for space group *Imma*, a cyclic permutation of the axes is needed, resulting in $a = 2c(CaCu_5)$, $b = \mathrm{sqrt}(3) * a(CaCu_5)$, and $c = a(CaCu_5)$. Both $EuPd_3Si_2$ and $SrPd_3Si_2$ crystallize in this (pseudohexagonal) *Imma* symmetry, retaining the basic features of the $CaCu_5$-type structure [see Figs. 1(a)–1(c)] [2,5,6,9,11]. The projection of the unit cell in the ab plane is shown in Fig. 1(a) and in the ac plane in Fig. 1(b) which shows that the multilayers of atoms are stacked along the a direction. The Pd atoms are arranged in puckered kagome-type layers, with Eu atoms coordinated by Pd and Si atoms in a pseudohexagonal arrangement [Figs. 1(a) and 1(c)]. The Eu (Sr) atoms are displaced from their ideal positions in the channels formed by the Pd and Si atoms, resulting in a slight zig-zag arrangement along the a axis [Fig. 1(c)]. The Si atoms are displaced from their ideal position (0,0,z), resulting in the formation of Si dumbbells, with Si-Si distances of 2.654 Å [1,22]. Lattice parameters and atomic positions for $EuPd_3Si_2$ and $SrPd_3Si_2$ are given in Tables I and II and details of the data collection and structure refinements have been deposited with the Fachinformationszentrum Karlsruhe, with ICSD CSD = 2 182 871 and 2 184 151. Due to these subtle structural distortions, the crystals are inherently twinned, indicating a possible structural phase transition at elevated temperatures.

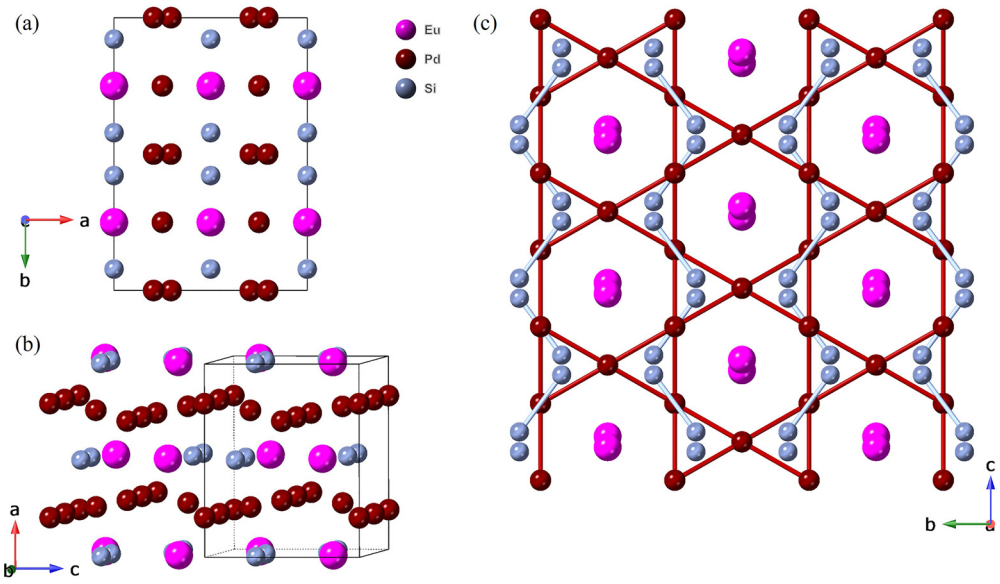

FIG. 1. Projection of the unit cell in (a) the *ab* plane, (b) the *ac* plane, and (c) the *bc* plane (oriented along the $CaCu_5$ *c* axis). The structure is twinned along a direction.

Figure 2 shows the Le Bail fit powder diffraction data of $EuPd_3Si_2$ and $SrPd_3Si_2$. The data clearly show the major orthorhombic *Imma* phase $EuPd_3Si_2$ ($SrPd_3Si_2$) with a minor amount of $EuPd_2Si_2$ ($SrPd_2Si_2$). Further data on refined lattice parameters from the powder samples are given in the Supplemental Material [23].

B. Physical properties

Single crystals of $EuPd_3Si_2$ were used for DC magnetic susceptibility measurements as a function of temperature and magnetic field. Figure 3(a) shows the temperature dependent zero field cooled DC susceptibility of a single crystal measured in 10 and 50 mT applied field. The field cooled susceptibility shown in Fig. 3(a) was measured with 10 mT. Two magnetic transitions are evident from the data, at $T_{C1} = 78$ K and $T_{C2} = 5$ K. As the sample cools and the temperatures reaches T_{C1}, the susceptibility sharply increases and then slightly decreases below T_{C1} resulting in a small dip before recovering almost to the same value at 78 K. It then stays almost constant down to T_{C2} with a slight enhancement below T^*. It further increases with decreasing temperature, followed by a second magnetic transition at $T_{C2} = 5$ K.

A small difference is also observed between the zero-field cooled and field cooled data. A weak feature is evident in the susceptibility data at $T^* = 30$ K. However, its origin cannot be discerned even from the NPD data. The inverse susceptibility data and Curie-Weiss fit are shown in the upper right inset of Fig. 3(a). In the temperature range from 80 to 300 K, the effective paramagnetic moment was found to be $\mu_{eff} = 8.25\,\mu_B/Eu^{2+}$, with a Weiss constant of $\Theta_C = 77.7$ K. The value of μ_{eff}. is slightly higher but not too far from the theoretically expected value for free Eu^{2+} spins ($7.94\,\mu_B$) only, while Θ_C matches very well with the FM ordering temperature of 78 K. The fact that the Curie-Weiss fit is linear close to T_{C1} indicates that spin fluctuations above T_C are negligible.

To further investigate the nature of these transitions, isothermal magnetization curves (M vs H) were measured on single crystals at four different temperatures, 2, 20, 50, and 300 K, and are shown in Fig. 3(b). The 300 K data are linear as expected for a paramagnet far above the ordering temperature. The magnetization saturates with magnetic field below T_{C1}, consistent with the dominant FM order with weak antiferromagnetic (AFM) correlation (canted AFM type) of Eu^{2+} spins at 78 K. However, the saturation moment at 20 and 50 K is significantly reduced compared to the expected saturation moment for Eu^{2+} spins that indicates that the ordering at 78 K is resulting from a canted AFM arrangement. Further the saturation moment at 2 K, below T_{C2}, increases and reaches the value of the expected moment for Eu^{2+}. A possible origin of this enhancement is explained by band structure calculations, which indicate that the Pd *d* bands are partially polarized

TABLE I. Structural data for $EuPd_3Si_2$: $a = 7.1483(4)$ Å, $b = 10.0743(4)$ Å, $c = 5.7506(2)$ Å, space group *Imma* (no. 74) (see also Table S1 in Supplemental Material [23]), $d_{calc} = 8.45\,g/cm^3$. Structural data have been deposited at ICSD with the CSD number 2182871.

Atom	Wyckoff positions	*x*	*y*	*z*	U_{eq}
Eu	4*e*	0	0.25	0.7154(2)	0.013
Pd1	8*f*	0.2950(1)	0	0	0.011
Pd2	4*c*	0.25	0.25	0.25	0.023
Si	8*h*	0	0.0786(5)	0.1852(8)	0.015

TABLE II. Structural data for $SrPd_3Si_2$: $a = 7.1807(2)$ Å, $b = 10.0924(3)$ Å, $c = 5.7786(2)$ Å, space group *Imma*, $d_{calc} = 7.34\,g/cm^3$. Structural data have been deposited at ICSD with the CSD number 2184151.

Atom	Wyckoff positions	x	y	z	U_{eq}
Sr	4*e*	0	0.25	0.7165(4)	0.020
Pd1	8*f*	0.2934(1)	0	0	0.016
Pd2	4*c*	0.25	0.25	0.25	0.037
Si	8*h*	0	0.0793(4)	0.1875(7)	0.015

(discussed below). Based on DC magnetization, the transition at $T_{C2} = 5\,K$ is proposed to be related to a possible spin reorientation. Additional DC magnetization measurements on the polycrystalline sample used in NPD studies are given in the Supplemental Material (Fig. S2) [23].

To investigate further the nature of the magnetic transitions, heat capacity measurements (C_p vs T) on $EuPd_3Si_2$ single crystals were performed as a function of temperature from 1.8 to 100 K and shown in Fig. 4(a). The data show two sharp λ-type transitions at $T_{C1} = 78\,K$ and $T_{C1} = 5\,K$, confirming that both transitions are associated with long range order of the Eu^{2+} spins. However, no apparent signature at T^* is observed in the heat capacity data. The heat capacity of the isostructural $SrPd_3Si_2$ was initially used as reference data to estimate the lattice contribution to the specific heat, and thereby isolate the magnetic entropy change ($\Delta S_{mag.}$) below T_{C1}. The calculated value of $\Delta S_{mag.} \approx 23.8\,J/mole\,K$ is roughly 37% percent higher than the expected value for Eu^{2+} spins ($\approx 17.3\,J/mole\,K$) [23]. Therefore, despite being isostructural and with an almost identical unit cell, $SrPd_3Si_2$ is not the best choice to estimate $\Delta S_{mag.}$ in $EuPd_3Si_2$. This is likely due to the mass difference between Sr and Eu that results in a different phonon spectrum for $SrPd_3Si_2$, rendering it less ideal as a reference material. Efforts to synthesize $BaPd_3Si_2$ were not successful. Therefore, we used a theo-

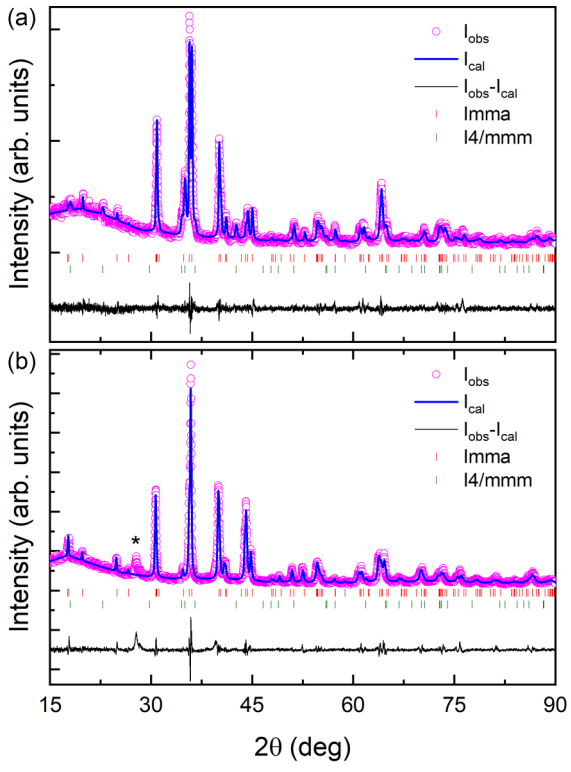

FIG. 2. Le Bail fit of XRD data from (a) $EuPd_3Si_2$ (*Imma*) and (b) $SrPd_3Si_2$ (*Imma*) using a two-phase model. The goodness of fit parameters is given in the respective figures. The peak marked with a star in (b) is due to Pd_2Si and excluded from the refinement. The refined lattice parameters are given in Table S1 in Supplemental Material [23].

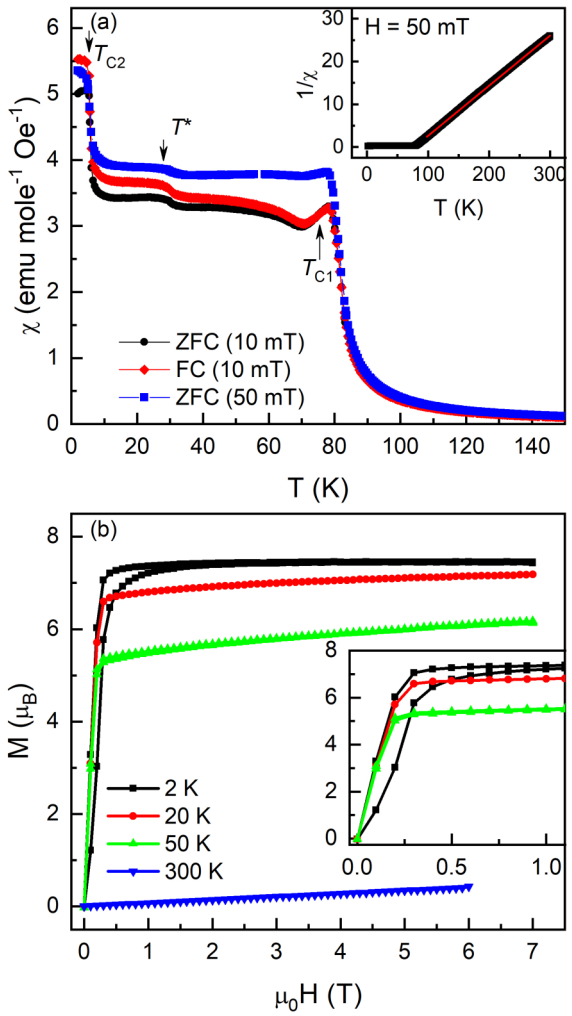

FIG. 3. (a) The ZFC DC magnetic susceptibility (χ vs T) of $EuPd_3Si_2$ single crystals measured with applied field 10 and 50 mT. The FC χ vs T was measured with 10 mT. The inset exhibits the Curie-Weiss fit of the inverse susceptibility data. (b) Magnetization vs field curves measured at 2, 20, 50, and 300 K.

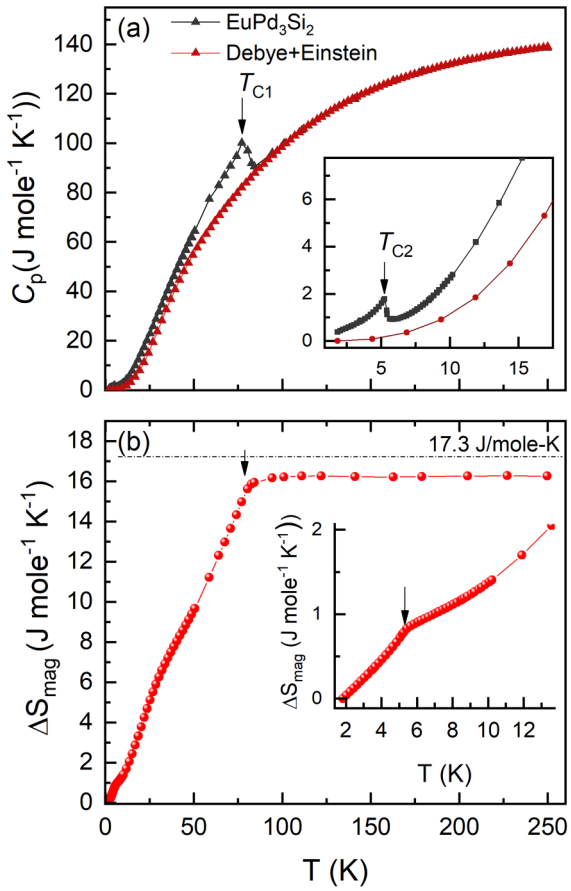

FIG. 4. Specific heat of single crystalline $EuPd_3Si_2$ as a function of temperature. The inset shows the enlarged view near the 5 K ordering. The estimated magnetic entropy using the Debye + Einstein model is shown in (b).

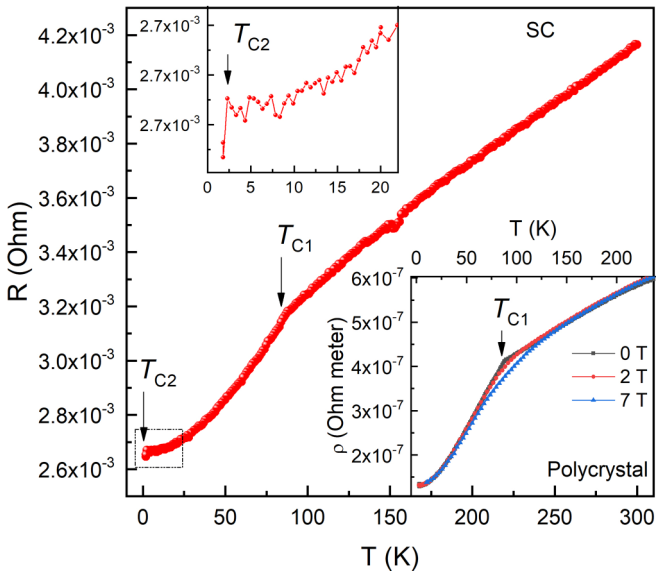

FIG. 5. Resistance vs temperature (R-vs-T) curve measured from the single crystal sample using four probe methods. The upper left inset shows the enlarged view of R-vs-T data near T_{C2}. The lower right inset shows the resistivity (ρ-vs-T) curves measured from the polycrystalline slab at different fields.

retical model with both Debye and Einstein components to estimate ΔS_{mag}. The resultant magnetic heat capacity and change in magnetic entropy are shown in Fig. 4(b). With this model, a Debye temperature of $\theta_D = 339$ K and Einstein temperature of $\theta_E = 283$ K are obtained, and as a result, the magnetic entropy contribution is $\Delta S_{mag.} = 16.25$ J/mole K, consistent with the expected value. Similar values of $\Delta S_{mag.}$ have been reported for other divalent Eu systems both in oxides [24] and alloys such as $EuCr_2As_2$, $EuMg_2Bi_2$, $EuGa_2Sb_2$, and $Eu_3In_2P_4$ [25–28].

Using only a Debye model, $\Delta S_{mag.}$ was again roughly 30% higher than expected. We ascribe the Einstein mode to the Pd_3Si_2 sublattice, with stronger bonding than the Eu atoms located in the channels of the structure. The magnetic contribution from Eu spins is primarily mediated through indirect Ruderman-Kittel-Kasuya-Yosida interactions.

To further investigate the effect of magnetic transitions on transport properties, electrical resistance (R)/resistivity (ρ) (R for single crystals and ρ for polycrystals) was measured on a single crystal and a polycrystalline slab of $EuPd_3Si_2$ using the four-probe method. As expected, both the single crystal and polycrystal samples show metallic behavior over the whole temperature range (see Fig. 5). The lower right inset shows the resistivity (ρ-vs-T) data measured on the polycrystalline sample as a function of temperature and for the magnetic field values of 0, 2, and 7 T. The resistivity measurement on the single crystal sample was hampered due to its small size and irregular shape whereas a reasonable value for the resistivity was obtained using the polycrystalline slab.

A small but clear change in resistance/resistivity is apparent at T_{C1} in both the single crystal and polycrystalline sample, showing a kink at the Curie temperature (T_{C1}) followed by a rapid decrease due to the reduction of spin disorder scattering. Further, we observe a small reduction of the electrical resistivity of the polycrystalline sample in the vicinity of T_{C1} on application of magnetic field, giving a small negative magnetoresistance. Only the single crystal data show a small drop in resistance at $T_{C2} = 5$ K as evident in the enlarged view in the upper left inset of Fig. 5. A possible reason is the better crystallinity and phase purity in single crystals as compared to polycrystalline materials. The R-vs-T curve of $SrPd_3Si_2$ confirms the metallic behavior and is given in the Supplemental Material [23].

C. Neutron powder diffraction studies

NPD experiments on Eu-containing compounds are hampered due to the very large absorption cross section of natural Eu [13–15], making magnetic structure investigations of Eu compounds by neutron diffraction/scattering difficult. Nevertheless, it was possible to obtain NPD patterns from our samples that contain the natural Eu isotope mixture, demonstrating that the brilliance of the POWGEN instrument is sufficient to overcome the severe constraints imposed by the large absorption cross section. In Fig. 6, we present the NPD patterns collected at $T = 1.6$, 30 and 67 K, which show magnetic diffraction intensities in the form of enhanced intensity of the nuclear reflections at large d spacings, such as 5.0, 2.87, 2.48 and 2.43 Å as compared to the 150 K data. Figure 6(b) depicts the difference patterns after subtracting the paramag-

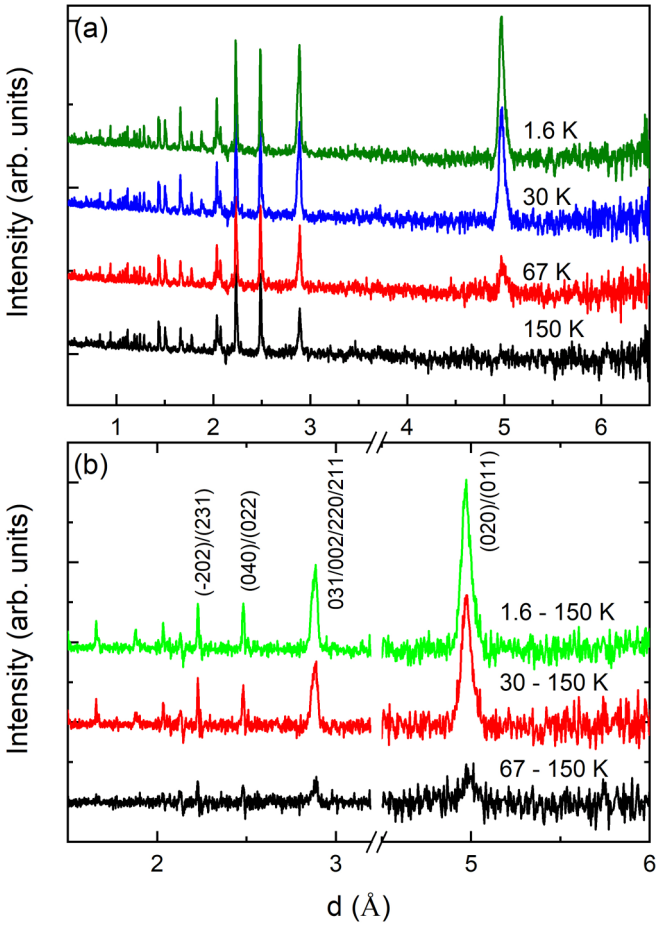

FIG. 6. (a) NPD patterns measured at different temperature using the POWGEN beamline and (b) the difference profiles after subtracting the paramagnetic contribution for 1.6, 30 and 67 K. The 150 K data is taken as a reference paramagnetic pattern to plot the difference profiles.

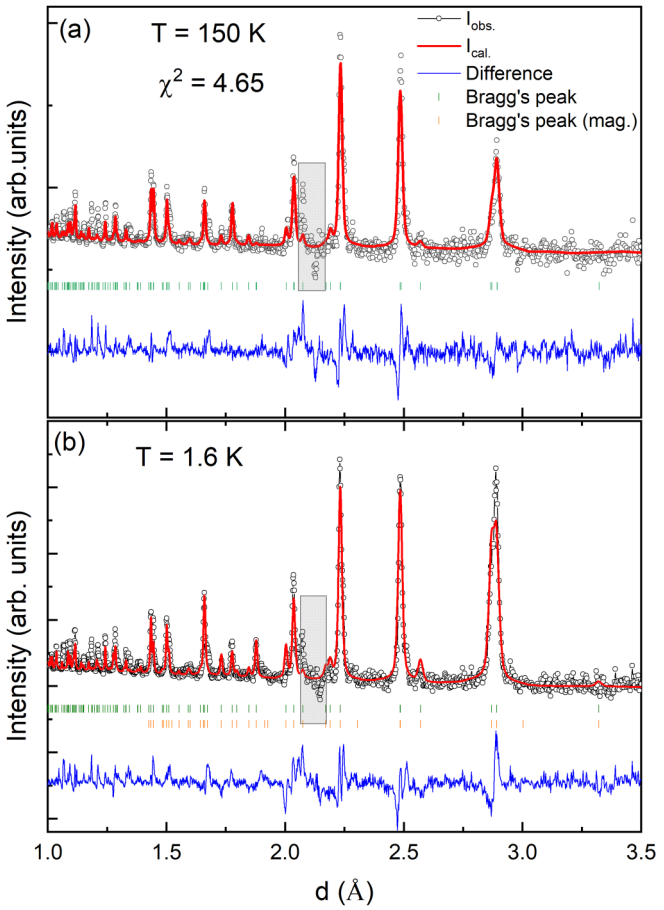

FIG. 7. Rietveld refined NPD pattern at (a) 150 K and (b) 1.6 K. At 1.6 K, the lower orange ticks represent the magnetic Bragg's positions where intensity is allowed in the FM state. Unindexed peaks at low d regions are due to $EuPd_2Si_2$ (see the text for more details). Regions with negative peaks are excluded from the refinement and shown within a hatched box.

netic contribution, i.e., the 150 K data. The remaining peaks can therefore be interpreted in terms of magnetic Bragg peaks occurring at the nuclear positions.

It is worth mentioning that the magnetic reflection with the highest intensity occurs near a d spacing of 5 Å where a nuclear reflection is allowed, but not observed at 150 K. All magnetic peaks occur at positions of allowed nuclear reflections. This confirms the long-range FM order of Eu^{2+} in $EuPd_3Si_2$ below 78 K. No additional peaks or features have been observed at 1.6 K (below T_{C2}) when compared to the 30 or 60 K data recorded (below T_{C1}). The NPD patterns are indexed using the magnetic propagation vector $\mathbf{k} = 0$ in which Eu^{2+} spins are situated at $4e$ position. The refined NPD patterns at 150 and 1.6 K are shown in Fig. 7.

Unindexed peaks in the lower d region stem from $EuPd_2Si_2$ that is present in the powder sample, as confirmed by Rietveld refinement of the powder XRD data. We performed a single-phase refinement for 150 K and a two-phase refinement of data at 1.6 K. It is important to mention here that in the minority phase $EuPd_2Si_2$, Eu exists in the Eu^{3+} state below 160 K, without magnetic order. The negative peak intensities arise from the subtraction of the vanadium peak of the PAC container from the high neutron absorbing sample and are excluded from the refinement and shown within a hatched box.

Based on the representational analysis, there are six possible solutions corresponding to the crystal structure out of which only the one having the moments along the a direction (along the c axis in the $CaCu_5$ prototype) is consistent with the data. The clear absence of the (200) reflection in the data is consistent with the refinement and supports the refined magnetic structure which is shown in Fig. 8.

The magnetic symmetry is determined as $Imm'a'$ where Eu^{2+} moments are aligned ferromagnetically along the a direction. An initial refinement gave an ordered moment value of $6\,\mu_B$/f.u., with the highest intensity reflection at 5 Å included. However, this value is considerably smaller than expected from the susceptibility measurement. While the magnetic Bragg peaks were generated at all expected positions, the lower d-spacing magnetic peaks' intensities were not well described, with only the strong high-d-spacing peak fitted properly. This can be more clearly seen in the difference fitting [23], that provides a more accurate estimation of the small changes in the magnetic structural parameters that are

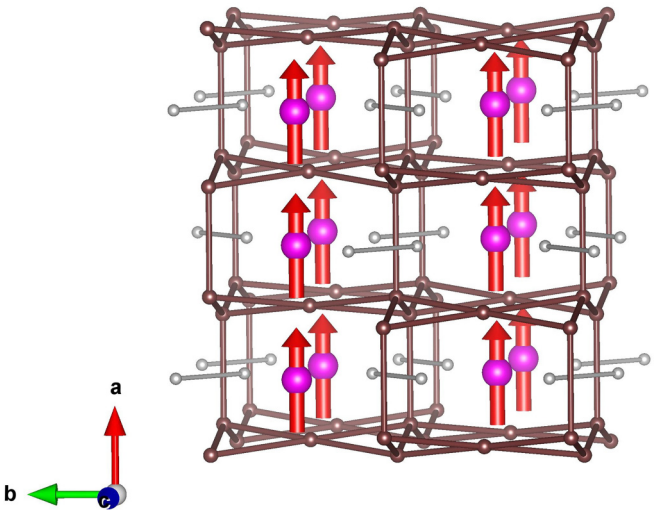

FIG. 8. Magnetic structure of $EuPd_3Si_2$ at 1.6 K. The pink sphere represents the Eu^{2+} atoms and the red arrows indicate the magnetic moment vector. The Pd-Pd kagome layers are shown with brown color atoms and bonds where the Si atoms are shown in gray color.

harder to detect in the raw powder data [29–31]. Thus, including the high d spacing peaks most affected by absorption led to a severe underestimation of the magnetic moment [23]. This is expected since the high d spacing peaks are mainly due to long neutron wavelengths. Excluding these high-d-spacing peaks from the refinement resulted in an ordered magnetic moment value of 8.0(2) μ_B/f.u., closer to the expected value. Such discrepancies due to the strong neutron absorption properties have also been observed for similar systems [13,14]. It was further suggested that even small amounts of strongly dispersed EuO impurities, undetected in NPD, could significantly affect the ordered magnetic state [14].

Also, based on the NPD data, the possibility of a canted spin arrangement below T_{C1} cannot be ruled out, perhaps reflected in the reduced saturation magnetization above T_{C2}. However, the strong neutron absorption of our sample rendered impossible the distinction between different models that include spin canting, and no further refinements of the data taken at temperatures in the range 5 K $< T <$ 78 K were pursued. Single crystal neutron diffraction studies on a sample synthesized with the Eu 153 isotope will be helpful to explore the origin of first magnetic transition at T_{C1}.

D. DFT calculations

The electronic structure calculations for both $EuPd_3Si_2$ and $SrPd_3Si_2$ yield similar band structures that indicate metallic behavior. The electronic densities of states and Pd d state projections are shown in Fig. 9, along with the Fermi surfaces of $SrPd_3Si_2$. The Eu f states are fully spin polarized in FM $EuPd_3Si_2$ as may be anticipated in a Eu^{2+} system. With the choice $U = 6$ eV, the occupied Eu $4f$ levels are narrow and centered at -1.4 eV relative to the Fermi level, E_F. The corresponding unoccupied minority spin $4f$ resonance is centered high above E_F at $+9$ eV. The main contributions to the valence electronic structure below E_F are from Si sp orbitals and Pd d orbitals. The shape and composition of the density of

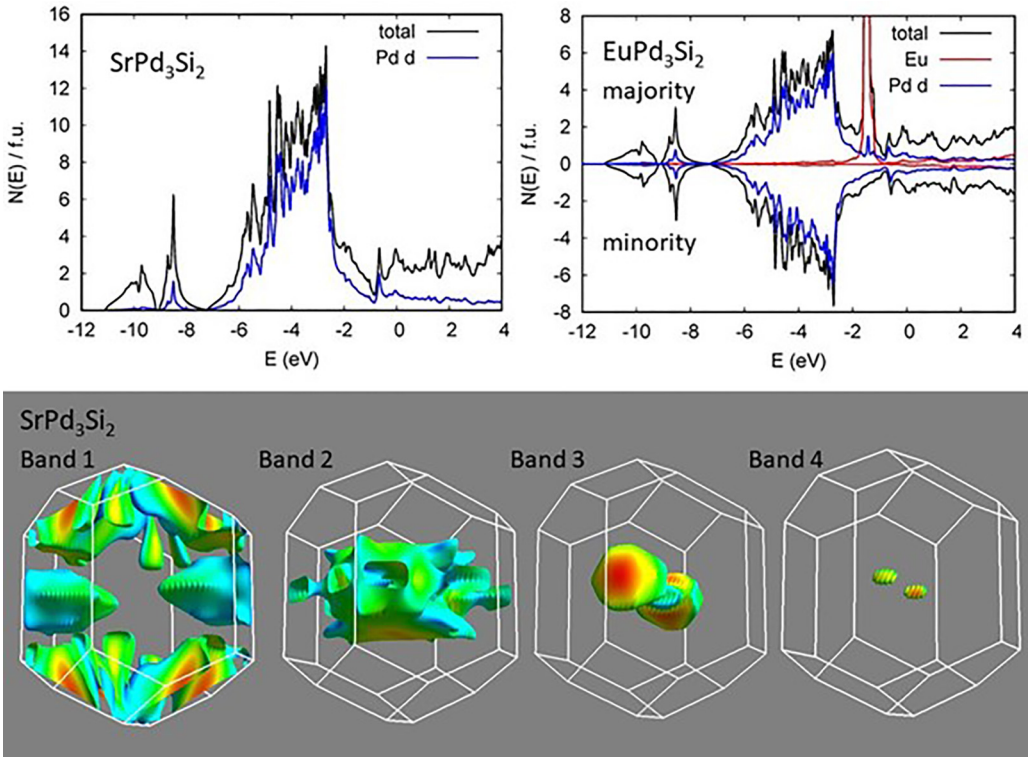

FIG. 9. Electronic density of states and projections of Pd d character for $SrPd_3Si_2$ and ferromagnetic $EuPd_3Si_2$ (top) and Fermi surfaces, shown in a perspective view with shading by velocity (blue is low velocity) for $SrPd_3Si_2$ (bottom). The Eu projection is also shown for $EuPd_3Si_2$. Projections are based on integration inside the LAPW spheres, which have a radius of 2.45 bohrs for Eu and Pd.

states are qualitatively similar to those of the group 10 Ni and Pd binary silicides [32,33]. Specifically, the electronic density of states shows a main Pd d band peak below the Fermi energy between ≈ -6 and -2 eV, but there is substantial Pd d character extending to E_F. This reflects considerable hybridization between Si sp and Pd d states. This hybridization, which favors high velocity bands, is known to be what gives these silicides their relatively high conductivity. The high velocity bands near E_F lead to modest absolute density of states at the Fermi level, $N(E_F)$, and therefore place these compounds far from Stoner instabilities towards magnetism.

We find $N(E_F) = 3.15\,\text{eV}^{-1}$ per formula unit for $SrPd_3Si_2$. This corresponds to a bare specific heat coefficient $\gamma_{\text{bare}} = 7.4\,\text{mJ/mol K}$ per formula unit. The Pd d contribution to $N(E_F)$ is $0.98\,\text{eV}^{-1}$ per formula unit ($\approx$0.33/Pd), as measured by the projections inside the Pd spheres. This is approximately 31% of the total. FM $EuPd_3Si_2$ is very similar except for an exchange splitting of the bands due to interactions with the Eu moments. We find $N(E_F) = 3.35\,\text{eV}^{-1}$, corresponding to $\gamma_{\text{bare}} = 8.0\,\text{mJ/mol K}$. The Pd d contribution is $\approx$33% of the total. The majority and minority spin contributions are $N_\uparrow(E_F) = 1.83\,\text{eV}^{-1}$ and $N_\downarrow(E_F) = 1.53\,\text{eV}^{-1}$. The actual specific heat coefficient is given by the bare band structure coefficient times an enhancement factor, $\gamma = \gamma_{\text{bare}}(1 + \lambda)$, where in simple metals λ is an electron-phonon coupling constant, and in materials near magnetism it may contain an additional contribution from spin fluctuations. Considering the structural and electronic similarity of $EuPd_3Si_2$ and $SrPd_3Si_2$, it may be expected that the electron-phonon enhancement would be similar. Thus, when suitable crystals become available it will be interesting to compare the specific heat enhancements to provide information about possible spin fluctuation contributions in $EuPd_3Si_2$.

The Fermi surfaces are large, multisheeted, and complex for both compounds. $SrPd_3Si_2$ (lower panel of Fig. 9) has four bands crossing E_F leading to four sheets of Fermi surface as shown. The Fermi surface is very three dimensional and there are no strong nesting features observed. The calculated values of σ/τ (conductivity divided by relaxation time) are 1.98×10^{20}, 1.99×10^{20}, and 3.25×10^{20} $(\Omega\,\text{ms})^{-1}$, for the a-axis, b-axis, and c-axis directions, respectively. The corresponding plasma frequencies are $\hbar\Omega_{\text{p,xx}} = 3.11$, 3.12, and 3.99 eV, respectively. Thus, the electronic transport is expected to be very isotropic in the ab plane and the conductivity is predicted to be somewhat higher along c. $EuPd_3Si_2$ is predicted to be similar with calculated values of 1.90×10^{20}, 1.99×10^{20}, and 3.11×10^{20} $(\Omega\,\text{ms})^{-1}$. As seen in Fig. 9, there is an exchange coupling between the Eu moments and the valence band electronic structure, leading to differences between the majority and minority spin densities of states. This implies a coupling between the Eu $4f$ derived moments and the Si-Pd derived bands. In $EuPd_3Si_2$, the net polarization of the valence bands is found to be in the same direction as that of the Eu $4f$ states, leading to an enhancement of the spin moment above the Eu f value of $7\,\mu_B$.

We calculate a value of $M_{\text{spin}} = 7.30\,\mu_B$ per formula unit. We additionally did test calculations including spin orbit coupling and find a similar value, with a small orbital moment per Eu of approximately $-0.01\,\mu_B$. Thus, there is an enhancement of the magnetization from polarization of the valence bands amounting to $\approx 0.30\,\mu_B$. This is qualitatively consistent with the magnetization measurements for the low temperature FM state, which also show a value higher than the nominal $7\,\mu_B$ [Fig. 3(b)].

IV. CONCLUSIONS

We have synthesized single crystals of the new compounds $EuPd_3Si_2$ and $SrPd_3Si_2$ using melt growth and Bridgeman techniques. The single crystal XRD refinement confirms that both compounds crystallize in the pseudohexagonal orthorhombic $ErRh_3Si_2$ structure with $Imma$ symmetry. In the crystal structure, the Pd atoms form puckered kagome-type layers, with Eu/Sr atoms located in between these layers and slightly offset from the ideal position expected from the prototype $CaCu_5$-type structure. The structural distortions lead to the formation of Si-Si dumbbells that break the hexagonal symmetry. $EuPd_3Si_2$ shows ferromagnetic order at $T_{C1} = 78$ K in addition to second transition at $T_{C2} = 5$ K. However, we cannot completely rule out the possibility of having a canted arrangement below T_{C1} which further undergoes full FM ordering below T_{C2}. The specific heat results confirm the long range order nature of both these transitions. The resistance vs temperature measurements confirm the metallic nature of these samples and in case of $EuPd_3Si_2$ the signature of magnetic ordering is clearly evident in the data. The ferromagnetic ground state at 1.6 K consists of Eu^{2+} spins aligned along the a directions (c direction in $CaCu_5$), perpendicular to the Pd kagome layers, consistent with DFT results. Within the available resolution range, we did not find any significant difference in the magnetic structures across T_{C1} and T_{C2}. It is very likely that the magnetic transition at 5 K is a spin reorientation transition from a canted arrangement, but it is impossible to confirm with our powder neutron diffraction measurements on this highly neutron absorbing sample.

ACKNOWLEDGMENTS

This work is supported by NSF Grant No. DMR-1625780. Part of the work was carried out at the National High Magnetic Field Laboratory, which is supported by NSF Grant No. DMR-1644779 and the State of Florida. Theoretical work at the University of Missouri was supported by the U.S. Department of Energy, Basic Energy Science, Grant No. DE-SC0019114. R.B. was supported by NSF Grant No. DMR-1904361. The research at the Spallation Neutron Source at Oak Ridge National Laboratory was sponsored by the Scientific User Facilities Division, Office of Basic Energy Sciences, U.S. Department of Energy.

[1] K. Cenzual, B. Chabot, and E. Parthé, $ErRh_3Si_2$ and isotypes with an orthorhombic deformation superstructure of the $CeCo_3B_2$ type, Acta Crystallogr. Sect. C **44**, 221 (1988).

[2] K. S. Athreya, L. S. Hausermann-Berg, R. N. Shelton, S. K. Malik, A. M. Umarji, and G. K. Shenoy, Superconductivity in the ternary borides $CeOs_3B_2$ and $CeRu_3B_2$: Magnetic

susceptibility and specific heat measurements, Phys. Lett. A **113**, 330 (1985).

[3] S. Seidel, R.-D. Hoffmann, and R. Pöttgen, $LaRh_3Ga_2$-structure determination from a trilling, Z. Anorg. Allg. Chem. **641**, 1400 (2015).

[4] B. Chevalier, A. Cole, P. Lejay, and J. Etourneau, New ternary silicides in rare earth-rhodium-silicon systems: Crystal structure and magnetic properties, Mater. Res. Bull. **16**, 1067 (1981).

[5] K. N. Yang, M. S. Torikachvili, M. B. Maple, and H. C. Ku, Intermediate valence behavior of ternary cerium and uranium transition metal borides, J. Low Temp. Phys. **56**, 601 (1984).

[6] A. M. Umarji, S. K. Dhar, S. K. Malik, and R. Vijayaraghavan, Evolution of magnetism from mixed-valent $CeIr_3B_2$ to Trivalent $CeIr_3Si_2$, Phys. Rev. B **36**, 8929 (1987).

[7] A. P. Pikul, D. Kaczorowski, Z. Gajek, J. Stępień-Damm, A. Ślebarski, M. Werwiński, and A. Szajek, Giant crystal-electric-field effect and complex magnetic behavior in single-crystalline $CeRh_3Si_2$, Phys. Rev. B **81**, 174408 (2010).

[8] S. K. Malik, S. K. Dhar, R. Vijayaraghavan, and W. E. Wallace, Magnetic and NMR Investigation of RRh_3B_2 (R = La to Gd) Compounds, J. Appl. Phys. **53**, 8074 (1982).

[9] K. N. Yang, M. S. Torikachvili, M. B. Maple, and H. C. Ku, Magnetic susceptibility of CeT_3B_2 and UT_3B_2 compounds (T = Co, Ru, and Ir), J. Appl. Phys. **57**, 3140 (1985).

[10] H. C. Ku, G. P. Meisner, F. Acker, and D. C. Johnston, Superconducting and magnetic properties of new ternary borides with the $CeCo_3B_2$-Type structure, Solid State Commun. **35**, 91 (1980).

[11] S. A. Shaheen, J. S. Schilling, P. Klavins, C. B. Vining, and R. N. Shelton, The anomalous magnetism of $CeRh_3B_2$ under pressure, J. Magn. Magn. Mater. **47–48**, 285 (1985).

[12] P. W. Betteridge, J. R. Carruthers, R. I. Cooper, K. Prout, and D. J. Watkin, *CRYSTALS* version 12: Software for guided crystal structure analysis, J. Appl. Crystallogr. **36**, 1487 (2003).

[13] W. N. Rowan-Weetaluktuk, D. H. Ryan, P. Lemoine, and J. M. Cadogan, Thermal neutron diffraction determination of the magnetic structure of $EuCu_2Ge_2$, J. Appl. Phys. **115**, 17E101 (2014).

[14] K. S. Nemkovski, D. P. Kozlenko, P. A. Alekseev, J.-M. Mignot, A. P. Menushenkov, A. A. Yaroslavtsev, E. S. Clementyev, A. S. Ivanov, S. Rols, B. Klobes, R. P. Hermann, and A. V. Gribanov, Europium mixed-valence, long-range magnetic order, and dynamic magnetic response in $EuCu_2(Si_xGe_{1-x})_2$, Phys. Rev. B **94**, 195101 (2016).

[15] Q. Zhang, J. Liu, H. Cao, A. Phelan, D. Graf, J. F. DiTusa, D. A. Tennant, and Z. Mao, Toward tunable quantum transport and novel magnetic states in $Eu_{1-x}Sr_xMn_{1-z}Sb_2$ ($z < 0.05$), NPG Asia Mater. **14**, 22 (2022).

[16] A. S. Wills, A New protocol for the determination of magnetic structures using simulated annealing and representational analysis (SARAh), Phys. B Condens. Matter **276–278**, 680 (2000).

[17] J. M. Perez-Mato, S. V. Gallego, E. S. Tasci, L. Elcoro, G. de la Flor, and M. I. Aroyo, Symmetry-based computational tools for magnetic crystallography, Annu. Rev. Mater. Res. **45**, 217 (2015).

[18] J. Rodríguez-Carvajal, Recent advances in magnetic structure determination by neutron powder diffraction, Phys. B Condens. Matter **192**, 55 (1993).

[19] P. Blaha, K. Schwarz, F. Tran, R. Laskowski, G. K. H. Madsen, and L. D. Marks, WIEN2K: An APW+lo program for calculating the properties of solids, J. Chem. Phys. **152**, 74101 (2020).

[20] J. P. Perdew, K. Burke, and M. Ernzerhof, Generalized Gradient Approximation Made Simple, Phys. Rev. Lett. **77**, 3865 (1996).

[21] G. K. H. Madsen and D. J. Singh, BOLTZTRAP. A code for calculating band-structure dependent quantities, Comput. Phys. Commun. **175**, 67 (2006).

[22] M. Dzevenko and I. Bigun, The new ternary silicide $ErCo_3Si_2$, Z. Naturforsch. B **69**, 369 (2014).

[23] See Supplemental Material at http://link.aps.org/supplemental/10.1103/PhysRevMaterials.7.023402 for [brief description].

[24] Y. Misawa, Y. Doi, and Y. Hinatsu, Magnetic ordering of divalent europium in double perovskites Eu_2LnTaO_6 (Ln = rare Earths): magnetic interactions of Eu^{2+} Ions determined by magnetic susceptibility, specific heat, and 151Eu mössbauer spectrum measurements, J. Solid State Chem. **184**, 1478 (2011).

[25] J. Jiang, M. M. Olmstead, S. M. Kauzlarich, H.-O. Lee, P. Klavins, and Z. Fisk, Negative magnetoresistance in a magnetic semiconducting zintl phase: $Eu_3In_2P_4$, Inorg. Chem. **44**, 5322 (2005).

[26] U. B. Paramanik, R. Prasad, C. Geibel, and Z. Hossain, Itinerant and local-moment magnetism in $EuCr_2As_2$ Single Crystals, Phys. Rev. B **89**, 144423 (2014).

[27] S. Pakhira, M. A. Tanatar, and D. C. Johnston, Magnetic, thermal, and electronic-transport properties of $EuMg_2Bi_2$ single crystals, Phys. Rev. B **101**, 214407 (2020).

[28] T. Berry, S. R. Parkin, and T. M. McQueen, Antiferro- and Metamagnetism in the S = 7/2 Hollandite Analog $EuGa_2Sb_2$, Phys. Rev. Mater. **5**, 114401 (2021).

[29] S. Sharma, D. T. Adroja, C. Ritter, D. Khalyavin, P. Manuel, G. B. G. Stenning, A. Sundaresan, A. D. Hillier, P. P. Deen, D. I. Khomskii, and S. Langridge, Magnetic ground state of the ordered double-perovskite Sr_2YbRuO_6: Two magnetic transitions, Phys. Rev. B **102**, 134412 (2020).

[30] S. Sharma, C. Ritter, D. T. Adroja, G. B. Stenning, A. Sundaresan, and S. Langridge, Magnetic structure of the double perovskite La_2NiIrO_6 investigated using neutron diffraction, Phys. Rev. Mater. **6**, 014407 (2022).

[31] D. T. Adroja, S. Sharma, C. Ritter, A. D. Hillier, D. Le, C. V. Tomy, R. Singh, R. I. Smith, M. Koza, A. Sundaresan, and S. Langridge, Muon spin rotation and neutron scattering investigations of the B-site ordered double perovskite Sr_2DyRuO_6, Phys. Rev. B **101**, 094413 (2020).

[32] Y. M. Yarmoshenko, S. N. Shamin, L. V. Elokhina, V. E. Dolgih, E. Z. Kurmaev, S. Bartkowski, M. Neumann, D. L. Ederer, K. Göransson, B. Noläng, and I. Engström, Valence band spectra of 4d and 5d Silicides, J. Phys. Condens. Matter **9**, 9403 (1997).

[33] A. Dahal, J. Gunasekera, L. Harringer, D. K. Singh, and D. J. Singh, Metallic nickel silicides: Experiments and theory for NiSi and first principles calculations for other phases, J. Alloys Compd. **672**, 110 (2016).